Materials Transactions, Vol. 51, No. 4 (2010) pp. 810 to 817

EXPRESS REGULAR ARTICLE

Effects of Rhenium on Microstructure and Phase Stability of MAR-M247 Ni-Base Fine-Grain Superalloy

Jian-Hong Liao[1,], Hui-Yun Bor[2], Chuen-Guang Chao[1] and Tzeng-Feng Liu[1]

[1]*Department of Materials Science and Engineering, National Chiao-Tung University, 1001 Ta-Hsueh Road, Hsin-Chu 30049, Taiwan, R. O. China*
[2]*Materials and Electro-Optics Research Division, Chung-Shan Institute of Science and Technology, Lung-Tan, Tao-Yuan 32599, Taiwan, R. O. China*

The effects of Re additions on the microstructure and phase stability of the cast fine-grain Mar-M247 superalloy were investigated in this study. The results showed that the grain sizes of the alloys with 0, 3, and 4.5 mass% Re content were 90, 60, and 50 μm, respectively. The primary γ' phase became finer and more cuboidal as Re content increased. The addition of 3 mass% Re caused strip-like MC carbides within the grain to degenerate into discontinuous $M_{23}C_6$ carbides and initiated the formation of a deleterious topological closed-packed (TCP) phase within the grain interior. The addition of 4.5 mass% Re promoted phase instabilities that led to the precipitation of large amounts of needle-like P phase in the grain interior, attributable to Re and W segregation. This study found that 3 mass% Re was a critical addition to maintain optimal microstructure and phase stability, and improved the ultimate tensile strength and the yield strength at room temperature and 760°C. However, the addition of 4.5 mass% Re obviously resulted in a decrease in tensile properties at room temperature and 760°C.
[doi:10.2320/matertrans.M2009331]

(Received September 30, 2009; Accepted January 25, 2010; Published March 10, 2010)

Keywords: *superalloy, rhenium, fine-grain, casting*

1. Introduction

Mar-M247 is a typical and well known nickel-base superalloy used in investment casting. Through its optimal alloy design and microstructure control, Mar-M247 superalloy has high strength and creep resistance at elevated temperatures. Basically, Mar-M247 consists of about 60% volume fraction of the γ' phase in the γ matrix, which is a solid solution strengthened by cobalt, molybdenum, tungsten, and chromium. Carbides have grain-boundary (GB) strengthening effects and also contribute to strength and ductility.[1–5] The fine-grain microstructure is beneficial for the strength and fatigue life of the superalloy at moderate temperatures (427–760°C). Thus, the fine grain process was developed for moderate temperature service.[6,7] Microcast-X, developed by Howmet Corporation, is a fine-grain technique with controlled low superheat and a high heat extraction rate.[7–9] This process offers the potential for producing cast with a fine-grain size of 65–125 μm.[8,9]

The strength of Ni-base superalloys is mainly determined by precipitates of the ordered intermetallic γ' phase in the γ matrix. Most related studies have reported a significant increase in strength with increasing γ' volume fraction and decreasing γ' size.[10] However, in modern Ni-base superalloys, the γ' phase is limited at 65–70% volume fraction for maximum precipitation hardening.[11] Adding solid solution elements, such as Re, W, Ta, and Mo, would further improve the strength of superalloys. On the other hand, the reliability of γ' for long-term exposures at elevated temperatures is another concern for superalloys, since the growth of γ' significantly degrades creep strength. Hence, recent studies have concentrated on adding refractory and slowly diffusing metals, such as Re and Ta, into the superalloy to retard the growth of γ'.[12]

Table 1 Crystallography of the TCP phases.

Phase	Until cell	*2Atoms per cell	*1Lattice constants (nm)		
			a	b	c
σ	tetragonal	30	0.880	—	0.454
P	orthorhombic	56	0.907	1.698	0.475
μ	rhombohedral	39	0.476	—	2.561
R	rhombohedral	159	1.090	—	1.954

*1The lattice constants of μ and R phases are defined on hexagonal axes.
*2Based on primary rhombohedral cell.

Previous studies have added 3 and 6 mass% Re in second- and third-generation single crystal superalloys, respectively, to improve their high-temperature mechanical properties.[13,14] Re is known to have effects that prevent γ' coarsening during thermal exposure and strengthen the γ matrix by a solid solution mechanism.[12–17] However, if the Re content is excessive, it tends to promote phase instabilities that lead to the formation of deleterious TCP phases, such as σ, P, μ, and R, during exposure to a high-temperature environment.[12,18–21] TCP phases are typically characterized by close-packed layers of atoms forming "basket weave" sheets, which are often aligned with the octahedral planes in the FCC matrix.[20,22] Table 1 summarizes the basic crystallography of common TCP phases.[18,21] Therefore, during the superalloy design process, the Re concentration must be controlled to stabilize the microstructure. However, until now, few studies have reported the effects of adding Re to fine-grain Ni-base superalloys.

This study investigates Mar-M247 superalloys with 0, 3, and 4.5 mass% additions of Re. It focuses on the effects of Re on microstructure and phase stability to determine the maximum allowable Re additions for the Mar-M247 superalloy.

Table 2 The chemical compositions of superalloys investigated (mass%).

Alloy	Mar-M247	alloy A (3Re)	alloy B (4.5Re)
Re	0	2.92	4.42
(Re at%)	(0)	(0.96)	(1.47)
Cr	8.35	8.42	8.40
Co	10.10	9.99	10.00
Mo	0.69	0.69	0.70
W	9.91	10.02	10.03
Ta	3.05	3.01	2.99
Al	5.42	5.33	5.37
Ti	1.0	0.98	0.97
Hf	1.32	1.29	1.22
C	0.15	0.14	0.14
B	0.02	0.02	0.02
Zr	0.04	0.04	0.04
Ni	bal.	bal.	bal.

Table 3 HIP cycle used in this study.

Temperature (°C)	25	→ 25 →	1135 →	1185 →	1185 →	*1300 →	*2RT
Pressure (MPa)	vacuum →	50 →	160 →	172.4 →	172.4 →	160 →	1 atm
Time interval (min)		50	165	30	240		

*1air (argon gas) quench
*2cooling in furnace

2. Experimental

In this study, 0, 3, and 4.5 mass% elemental Re were added to Mar-M247 superalloy and named as Mar-M247, alloy A (3Re), and alloy B (4.5Re), respectively. Mar-M247 superalloy and the Re addition were melted in a vacuum furnace and then cast into test bars using the Microcast-X process, which is a fine-grain technique with a low pouring temperature. The temperature gradient in the Microcast-X process was reduced to limit grain growth. The pouring and mold temperatures were 1380°C and 1100°C, respectively. Table 2 gives the original alloy compositions used in this study. The chemistries of each alloy were determined using X-ray fluorescence (XRF) except for the Re content, which was determined by inductive coupled plasma (ICP) chemical analysis. Hot isostatic pressing (HIP) was executed at 1185°C under gaseous Ar at a pressure of 172.4 MPa for 4 h (HIP cycle is shown in Table 3). A heat treatment of solid solution was carried out at 1185°C/2 h in vacuum, followed by cooling in argon gas. Samples were subjected to aging heat treatment at 871°C/20 h and then cooled to room temperature in the furnace.

Grain sizes were measured by determining the mean linear intercept of the grains in optical microscopy (OM). Field emission scanning electron microscopy (SEM) was adopted to characterize the microstructures. Energy dispersive spectroscopy (EDS) was used to determine the composition of various phases. Transmission electron microscopy (TEM) was used to determine the crystal structure of carbide and the TCP phase. The distribution of elements was determined using electron probe microanalysis (EPMA) map. The differential thermal analysis (DTA) method was used to investigate the effect of Re on alloy solidus and liquidus temperatures. All DTA tests were performed at a heating rate of 5°C/min in argon gas using alumina crucibles. Tensile tests were performed using an Instron 1125 universal test machine with 0.2 mm/min withdrawal speed at room temperature (RT) and 760°C in atmosphere. For the 760°C tensile tests, the test bar was heated to 760°C at a heating rate of 10°C/min and then held for 30 min to test. The gauge size of all test bars was 6.3 mm in diameter and 26 mm in length.

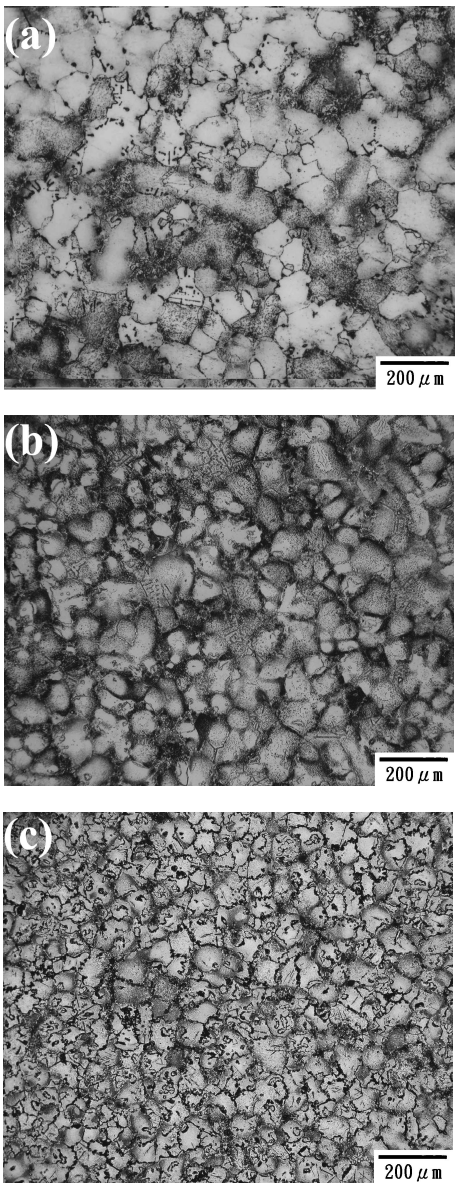

Fig. 1 OM of (a) Mar-M247, (b) alloy A (3Re), and (c) alloy B (4.5Re) after heat treatment.

3. Results

3.1 Microstructures

Figure 1 displays the grain size of the three superalloys after heat treatment. The average grain sizes of Mar-M247, alloy A (3Re), and alloy B (4.5Re) were 90, 60, and 50 μm, respectively. Clearly, increasing the Re content reduced grain size.

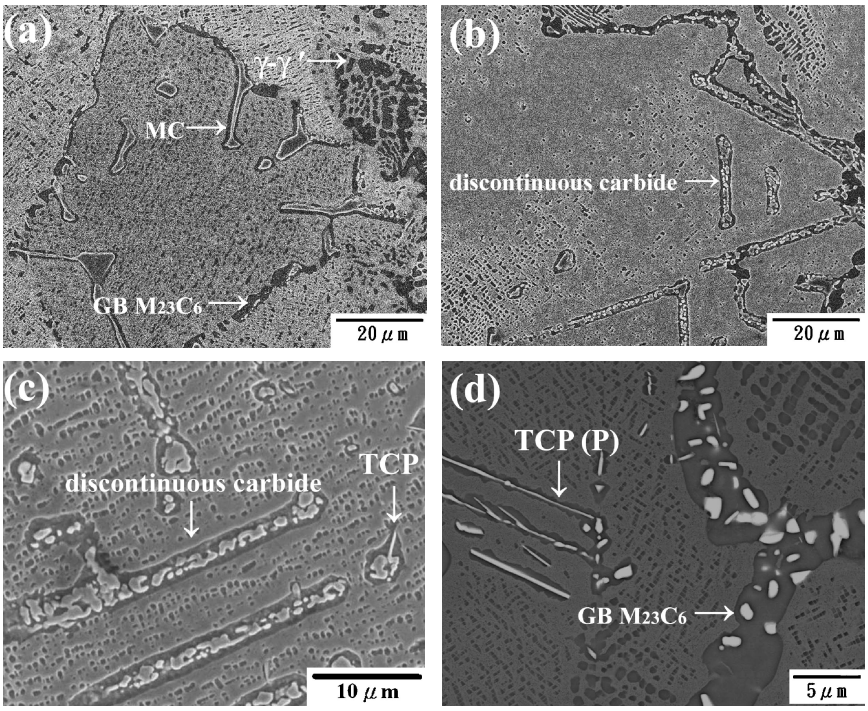

Fig. 2 SEM microstructures of (a) Mar-M247, (b) alloy A (3Re), (c) TCP phase formation in alloy A (3Re), and (d) alloy B (4.5Re) (BSE images) after heat treatment.

Table 4 Chemical compositions of various phases in these alloys given by EDS (at%).

	MC carbide (see Fig. 2(a))	GB $M_{23}C_6$ carbide (see Fig. 2(a))	discontinuous carbide (see Fig. 2(b))	TCP phase (see Fig. 2(c))	P phase (see Fig. 2(d))	GB $M_{23}C_6$ carbide (see Fig. 2(d))
elements	Mar-M247	Mar-M247	alloy A	alloy A	alloy B	alloy B
C	36.9	15.2	19.9	19.0	6.7	16.7
Al	4.0	4.6	4.8	6.3	9.2	5.3
Hf	6.9	0.0	1.0	0.4	—	—
Ta	24.8	5.7	7.1	1.4	0.5	2.8
W	7.5	26.3	15.0	12.3	15.8	20.8
Re	—	—	6.3	8.8	11.2	12.8
Mo	1.1	2.1	—	—	1.5	1.2
Ti	12.6	1.2	2.8	0.7	1.2	—
Cr	1.4	9.2	8.1	10.5	10.7	11.9
Co	1.0	7.4	7.9	7.9	8.4	7.9
Ni	3.8	28.3	27.1	32.7	34.8	20.6

Figure 2 and Table 4 show the microstructure and EDS analysis of the three superalloys. Following the previous studies of Mar-M247 microstructures,[1–5] the microstructures of the original Mar-M247 superalloy indicated that the main phases comprised (1) the γ matrix, (2) the reinforced phase γ', (3) the rosette eutectic structure γ-γ', (4) strip-like MC carbides within the grain interior and (5) particle carbides at the GB (Fig. 2(a)). The MC carbides in the grain interior were 10∼20 μm long. In addition, EDS analysis of MC carbides indicated that they were rich in Ta and Ti. On the other hand, the particle carbides existing at the GB had a size of 0.5∼1 μm, and EDS analysis indicated that they were rich in Cr and W. The particle-like carbide was identified as FCC $M_{23}C_6$ carbide with a lattice constant of 1.05 nm by TEM (Fig. 3). The microstructure of alloy A (3Re) revealed that discontinuous carbides were formed in the grain interior. The discontinuous carbides, with individual size of 0.5∼1 μm, contained high levels of Cr and W elements (see Table 4) and lined up to form structures 10∼20 μm in length, as shown in Fig. 2(b). Figure 2(c) shows a short needle-like precipitate that formed on the discontinuous carbides in alloy A (3Re). EDS measurements indicated that the precipitate had high Re and W contents (see Table 4). Therefore, it should be identified as a TCP phase by its needle-like shape and high Re and W contents. In this research, few needle-like TCP phases were observed in alloy A (3Re). Figure 2(d) is a back-scattered electron (BSE) micrograph of alloy B (4.5Re). In this mode, phases that are typically enriched with regard to heavy elements, such as Re and W, are clearly distinguishable against a dark background consisting of the γ and γ' phases. The needle-like precipitates (bright) were observed on particle carbides or in the vicinity of particle carbides

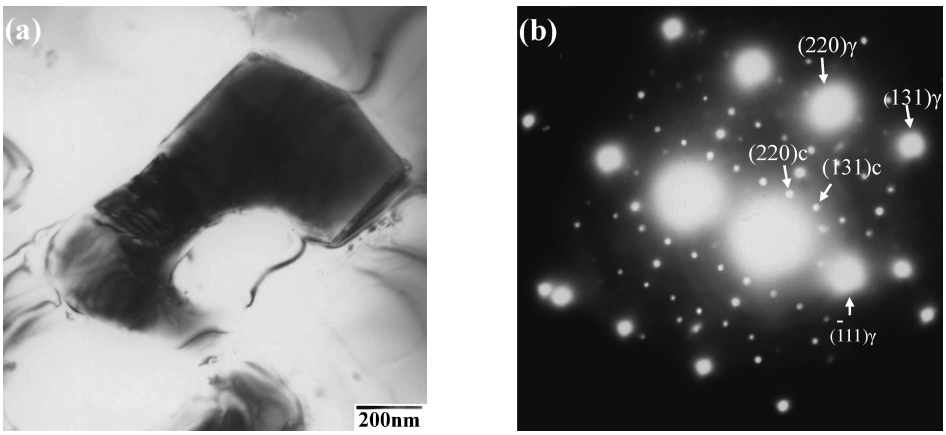

Fig. 3 (a) TEM bright-field image of the $M_{23}C_6$ carbide and (b) selected area diffraction pattern (SADP) with [1$\bar{1}$2] zone in Mar-M247. Subscripts c and γ refer to the carbide and γ matrix.

within the grain interior. The needle-like precipitates were 10–20 μm long, and EDS measurements indicated that they had high Re and W contents (see Table 4). TEM identified the needle-like precipitates as the orthorhombic P phase (Fig. 4). The GB carbides reveal bright contrast, suggesting that they also contained high levels of heavy elements, and EDS measurements indicated that they had high Re and W contents (see Table 4). The morphologies of GB carbides of various Re-containing superalloys were very similar.

Figure 5 shows the morphology of γ' precipitates. Both the primary block γ' and the secondary γ' phases were distributed in the matrix of Mar-M247. However, primary block γ', primary cube γ', and secondary γ' phases were observed in alloy A (3Re). Finally, alloy B (4.5Re) contained primary cube γ' and the secondary γ' phase. The size of primary block γ', primary cube γ', and secondary γ' were about 0.8, 0.3, and 0.05 μm, respectively.

3.2 The distribution of elements

EPMA maps were obtained for the as-heated samples. In Mar-M247, the result indicated that the elements Ta, Ti, and Hf were partitioned heavily to the MC carbide, while W appeared to be uniformly distributed (Fig. 6). In alloy B (4.5Re), the elements of Re and W partition heavily to the P phase and GB carbide, while Ta, Ti, and Hf exhibit a low degree of segregation to partial GB carbide (Fig. 7). The area of γ matrix reveals uniform but lower concentrations of Re and W distribution.

3.3 DTA results

Figure 8(a) plots the DTA curves of Re-free and Re-containing samples. All tests were performed on the as-heated sample. Each solidus temperature measurement was resolved by using the onset temperature for the endothermic liquidus peak. The corresponding liquidus temperature was resolved as the maximum endothermic peak value.[23] The solidus and liquidus temperatures are shown in Fig. 8(b). The DTA results reveal that the liquidus temperatures of Mar-M247, alloy A (3Re), and alloy B (4.5Re) were 1363°C, 1365°C, and 1367°C, respectively. On the other hand, the solidus temperatures of Mar-M247, alloy A (3Re), and alloy B (4.5Re) were 1324°C, 1329°C, and 1331°C, respectively.

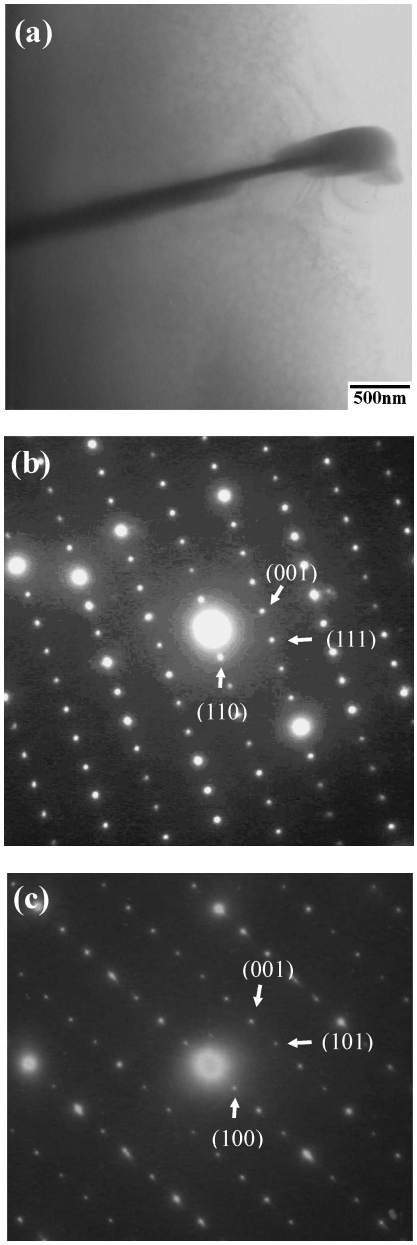

Fig. 4 (a) TEM bright-field image of the P phase, (b) SADP with [1$\bar{1}$0] zone, and (c) SADP with [010] zone in alloy B (4.5Re).

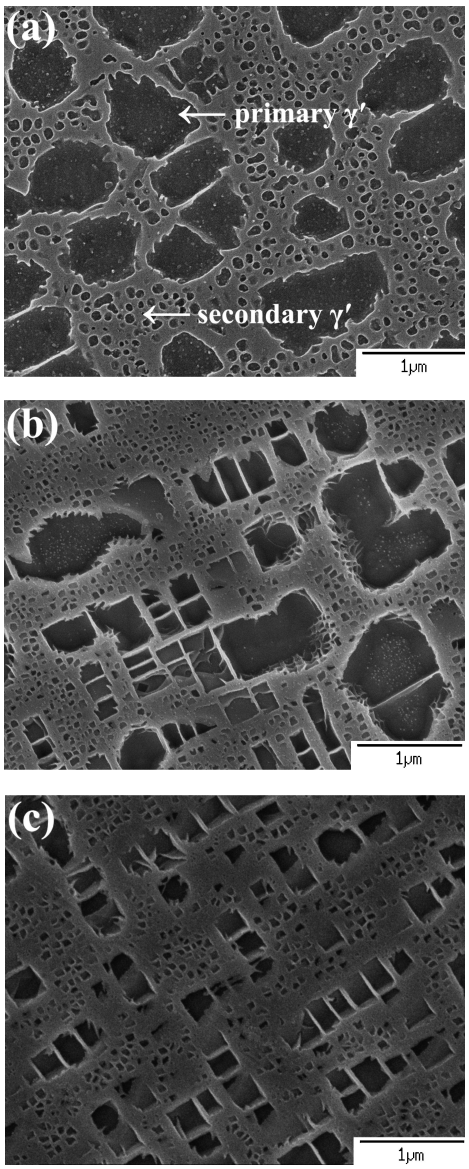

Fig. 5 γ' phase morphology of (a) Mar-M247, (b) alloy A (3Re), and (c) alloy B (4.5Re).

The DTA results indicated that the solidus and liquidus temperatures both increased with Re content.

3.4 Tensile properties

Figure 9(a) shows engineering stress-strain curves for Mar-M247. The tensile properties of Mar-M247 superalloy with various Re contents tested at RT and 760°C are given in Fig. 9(b)–(d). In the results of the RT test, the ultimate tensile strength (UTS), 0.2% offset yield strength (YS), and elongation (EL) of Mar-M247 were 1119 MPa, 980 MPa, and 4.8%, respectively. Alloy A (3Re) exhibited the best UTS, YS, and EL, which were 1200 MPa, 1056 MPa, and 5.4%, respectively. In contrast, the UTS, YS, and EL of alloy B (4.5Re) were decreased to 1105 MPa, 949 MPa, and 2.4%, respectively. In the results of the 760°C test, the tensile properties exhibited a similar tendency to those in the RT test. Alloy A (3Re) exhibited the best UTS, YS, and EL which were 1220 MPa, 1071 MPa, and 5.8%, respectively. In contrast to Mar-M247, the UTS, YS and EL of alloy A (3Re) were increased by 6.2%, 7.1%, and 11.5% at 760°C, respectively. However, alloy B (4.5Re) displayed the lowest tensile properties.

4. Discussion

4.1 Effect of Re content on grain size

Studies have reported that adding the high melting temperature element Re to multicomponent Ni-base alloys can increase the melting temperature.[15,24] In this study, similar results were obtained: adding Re increases the solidus and liquidus temperatures of the Mar-M247 superalloy. It has been shown that crystal growth is dependent on solid/liquid interface diffusion in the solidification of metal.[25] For the Microcast-X process, a lower superheat of melting alloy which has a shorter solidification time to allow atoms to leave the liquid and join the crystal, therefore limits the grain growth. Thus, under some pouring temperatures, a higher melting temperature alloy with the lower superheat of the melting alloy limits the grain growth and yields a finer-grained microstructure.

4.2 Effect of Re content on γ' phase

This study demonstrates that adding Re can prevent the primary cube γ' phase from coarsening to the primary block γ' phase. The γ' coarsening is mainly controlled by the diffusion of γ' formation elements, such as Al and Ti, to the γ' phase.[16,26,27] Previous studies have shown that Re inter-diffuses slowly in Ni. Atom probe investigations have shown pileup of Re solute atoms in the γ matrix ahead of the growing γ' phase.[15,16,27,28] Thus, the added Re that segregates at the γ/γ' interface will reduce the growth rate of the γ' phase by inhibiting the diffusion of Al and Ti to the γ' phase. Therefore, the primary γ' phase becomes finer as the Re content increases. A spherical γ' phase was observed with a near-zero γ/γ' lattice misfit, whereas misfit increased the tendency for formation of γ' phase with a cuboidal shape.[29] Re partitions in the γ matrix and causes high lattice misfit by its large atomic radius.[15,28] Thus, the shape of primary γ' phases were translated from block (near spherical) to cubical as more Re was added.

4.3 Effect of Re content on carbides and TCP phase

The compositions of strip-like MC carbide at the grain interior of Mar-M247 were mainly TaC and TiC. Ta and Ti had been reported to strengthen binding forces to such an extent that they make MC carbide degrade very slowly during exposure to high temperatures. Therefore, HIP and solution treatment, which were executed at 1185°C, cannot cause stable TaC and TiC to degrade in Mar-M247. However, the concentration of Ta and Ti in MC carbide of the grain interior fell as more Re was added. MC carbides were replaced by discontinuous carbides in alloy A (3Re). In previous report, $M_{23}C_6$ carbide has moderate to high Cr content.[1,2,7] The carbon content of the discontinuous carbide is close to the theoretical value of $M_{23}C_6$ (20.7 at%) and has moderate Cr content. Therefore, the discontinuous carbide should be the $M_{23}C_6$ carbide. An earlier investigation showed that MC carbide degenerated to $M_{23}C_6$ carbide over 980°C.[30] The reaction can be expressed as:

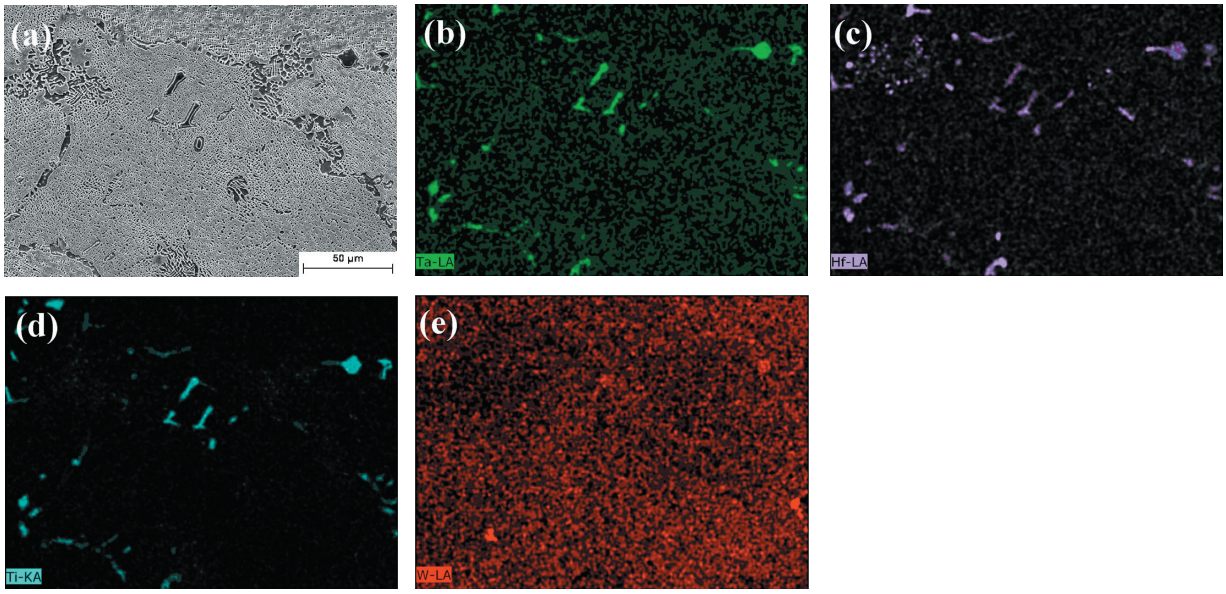

Fig. 6 (a) SEM image of Mar-M247 and (b) EPMA maps of Ta, (c) Hf, (d) Ti, and (e) W.

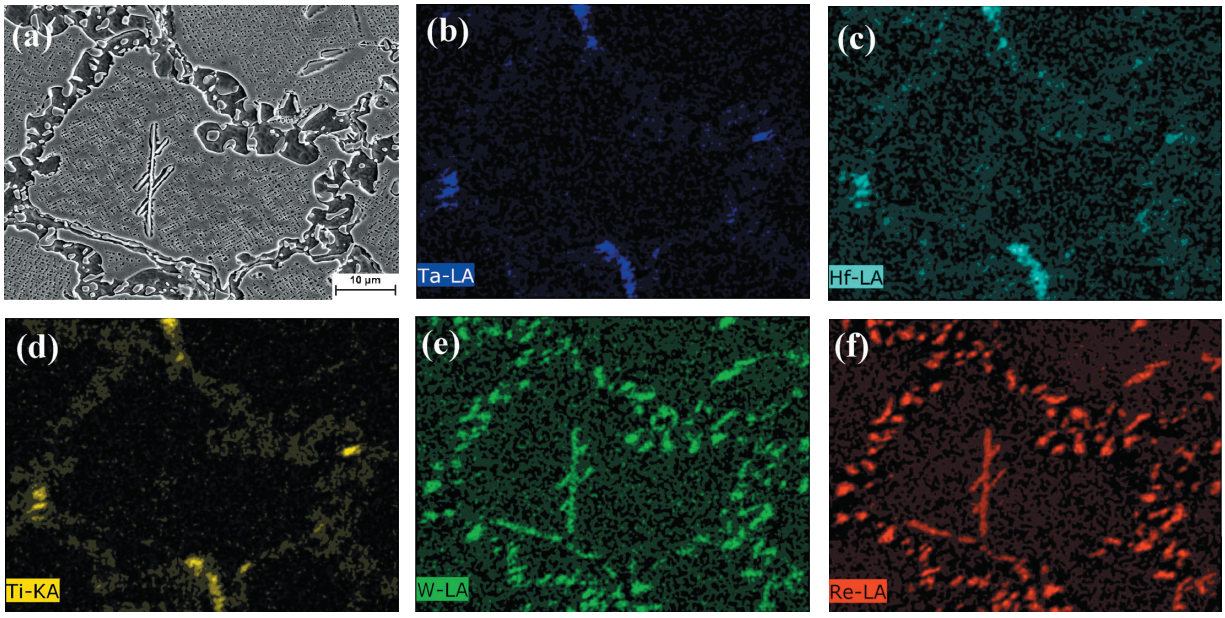

Fig. 7 (a) SEM image of alloy B (4.5Re) and (b) EPMA maps of Ta, (c) Hf, (d) Ti, (e) W, and (f) Re.

$$MC + \gamma \rightarrow M_{23}C_6 + \gamma'$$

The HIP and solution heat treatment used herein were performed over 980°C. Moreover, the amount of stable TaC and TiC carbides decreased as Re increased; therefore, unstable strip-like MC carbide degraded to discontinuous $M_{23}C_6$ carbide in alloy A (3Re). To the authors' experiment, MC carbide degraded to discontinuous $M_{23}C_6$ during the HIP process in alloy A (3Re) (not shown in SEM). This reaction has also been reported in another Re-containing fine-grain superalloy (CM-681LC).[7)]

Previous researches showed that TCP phases might form if the refractory element concentration was too high (over 17 mass%) in the alloy.[12–18)] In this study, few needle-like TCP phases formed on the discontinuous $M_{23}C_6$ carbide in alloy A (3Re), indicating that the addition 3 mass% Re caused the TCP formation elements, such as Re and W, to segregate to the discontinuous $M_{23}C_6$ carbide at the critical level. Previous studies have also shown that the σ phase is the first TCP phase formed, and it provides nucleation sites for the other TCP phases. The σ phase is not the most thermodynamically stable; depending on the alloy composition, other TCP phases are formed from it.[18)] Due to the low diffusivities of Re and W in Ni at elevated temperatures, the residual segregation of high levels of Re and W tends to form the P phase.[20)] Indeed, large amounts of P phases appeared in alloy B (4.5Re). The P phase contained a large amount of refractory metal elements, including Re, W, Hf, Ta, and Mo, the total amount of refractory elements is 29 at%, as shown in Table 4. The segregation of excessive

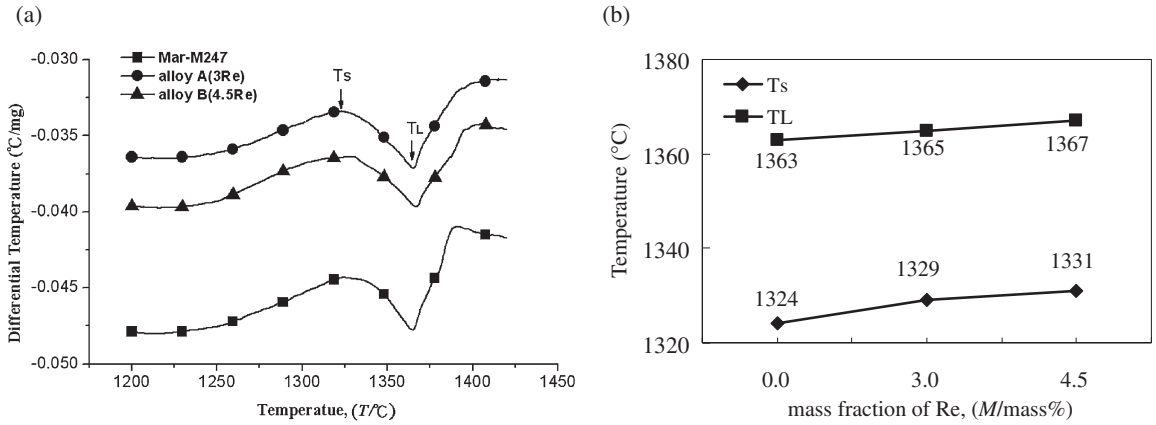

Fig. 8 (a) The DTA curves and (b) melting temperature (Ts: solidus temperature; TL: liquidus temperature) of various Re-containing Mar-M247.

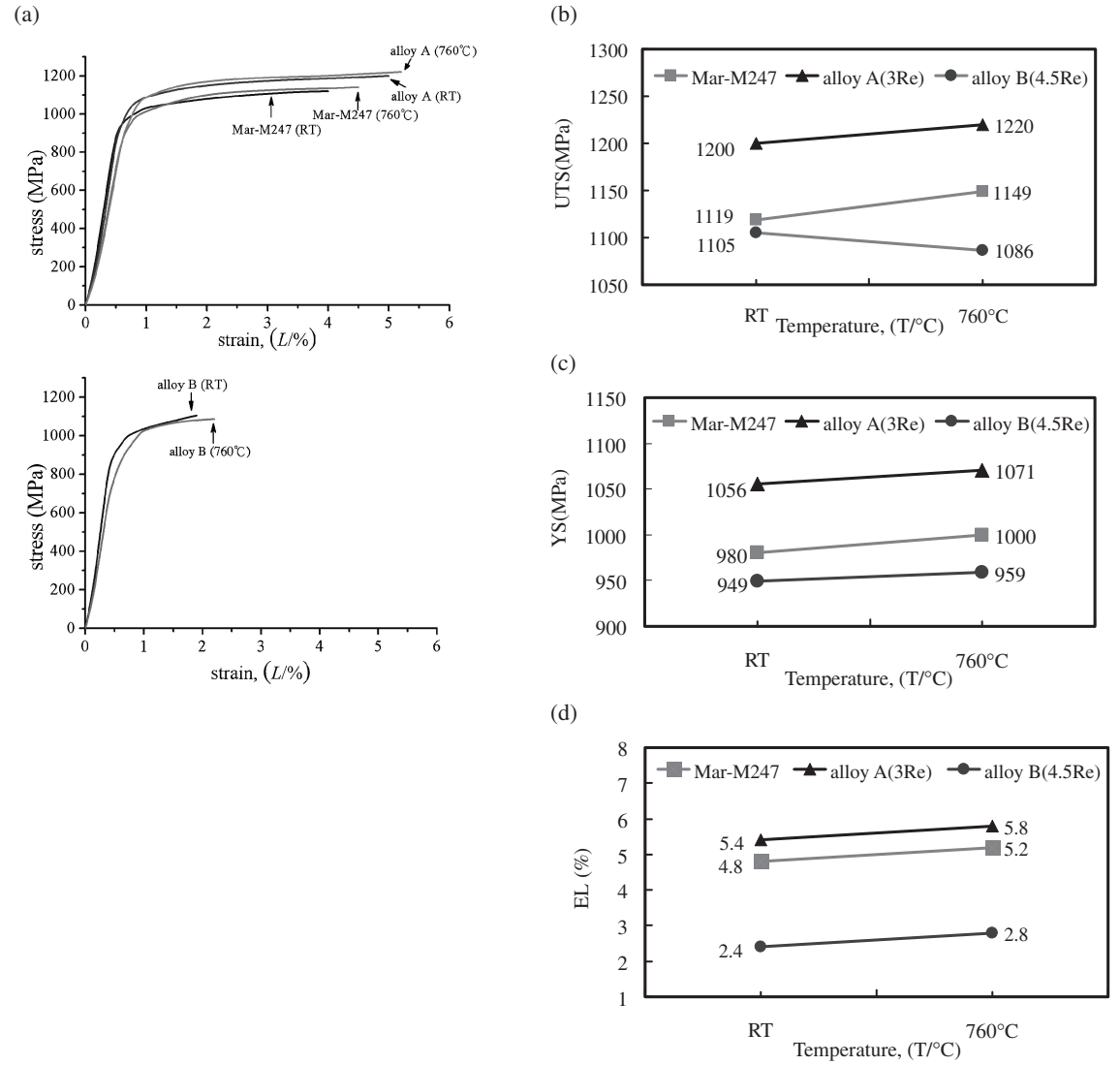

Fig. 9 The tensile properties of Mar-M247 superalloy with various Re contents tested at RT and 760°C. (a) engineering stress-strain curves, (b) ultimate tensile strength (UTS), (c) 0.2% offset yield strength (YS), and (d) elongation (EL).

refractory metal elements, especially for Re and W, promotes the formation of the stable P phase rather than other types of TCP phases. This study has demonstrated that Re and W play a pivotal role in the mechanism of P phase formation in this alloy. This result is consistent with other studies of Re-containing superalloy; however, the formation of the P phase should be prevented. It is noticed that no needle-like TCP phase was observed at GBs in alloy B (4.5Re), although the GB carbide contained large amounts of refractory metal elements. A study has reported that Hf and B concentrated at GBs can inhibit the formation of TCP phases,[26] but the detailed mechanisms are still unclear.

Thus, more studies should be performed to examine this phenomenon.

4.4 Effect of Re on tensile properties

According to the results of tensile testing at RT and 760°C, alloy A (3Re) exhibited the best UTS and YS. In contrast, adding 4.5 mass% Re decreases of tensile properties. Generally, the strength of an alloy is very dependent on grain size. According to the Hall-Petch equation, the strength is a function of the reciprocal of the square root of the grain size below about 0.5 Tm, where Tm is absolute melting temperature.[31] It is well known that the amount, size, and distribution of the γ' phase in superalloys considerably affects the tensile properties. Most studies have shown that strength increases as the size of the γ' phase decreases. Re is known to be a potent solid solution strengthener. Therefore, the addition of 3 mass% Re, which promotes the tensile properties, contributes to the Re solution strength effect and the refinement of grain size and γ' phase. Although, alloy B (4.5Re) showed the highest Re content and the finest grain and γ' phase size, it showed the lowest tensile properties in this study. There must be other factors causing the drop in strength of alloy B (4.5Re). The presence of TCP phases was reported to result in significantly decreased ductility and strength in two ways. First, its brittle and needle-like morphology is an excellent source for crack initiation and propagation leading to brittle failure. Also, the formation of TCP phases results in a decrease in solution-strengthening metal content in the matrix.[18,19,26] Indeed, the formation of the P phase depleted the surrounding matrix of solution-strengthening elements, such as Re, W, and Cr, in this study. Therefore, the formation of the needle-like P phase appears to be a major contributing factor for deterioration of tensile properties in alloy B (4.5Re).

5. Conclusions

The effects of Re addition on the microstructure and phase stability of cast fine-grain Mar-M247 superalloy herein are summarized as follows:

(1) The sizes of grains with 0, 3, and 4.5 mass% Re additions are 90, 60, and 50 μm, respectively, indicating that Re addition reduces grain size.
(2) The primary γ' phase becomes finer and more cuboidal as Re content increases.
(3) With 3 mass% Re addition, strip-like MC carbides within the grain degenerate into discontinuous $M_{23}C_6$ carbides. Rare few needle-like TCP phases were observed in the grain interior; therefore, 3 mass% Re is critical to initiating the formation of the TCP phase.
(4) With 4.5 mass% Re addition, EPMA and EDS analysis revealed that the Re and W concentrated at the P phase and GB carbide. The segregation of Re and W caused phase instabilities that led needle-like P phases to form in the grain interior, but no needle-like TCP phase formed at the GB.
(5) Adding 3 mass% Re to Mar-M247 superalloy improved the UTS and YS at RT and 760°C. In contrast, adding 4.5 mass% Re obviously resulted in a decrease of tensile properties at RT and 760°C.

Acknowledgments

The authors would like to thank Mr. Y. P. Huang for his help in mechanical property evaluation. The equipment support of processing from Mr. G. D. Cai and Dr. J. Y. Wang is also thankfully acknowledged.

REFERENCES

1) H. Y. Bor, C. G. Chao and C. Y. Ma: Metall. Trans. A **30A** (1999) 551–561.
2) H. Y. Bor, C. G. Chao and C. Y. Ma: Metall. Trans. A **31A** (2000) 1365–1373.
3) M. V. Nathal, R. D. Maier and L. J. Ebert: Metall. Trans. A **13A** (1982) 1767–1774.
4) H. Y. Bor, C. G. Chao and C. Y. Ma: Scr. Mater. **38** (1998) 329–335.
5) M. V. Nathal, R. D. Maier and L. J. Ebert: Metall. Trans. A **13A** (1982) 1775–1782.
6) C. T. Sims, N. S. Stoloff and W. C. Hagel: *Superalloys II*, (John Wiley & Sons, New York, 1987) pp. 420–426.
7) C. N. Wei, H. Y. Bor and L. Chang: Mater. Trans. **49** (2008) 193–201.
8) Lin Liu, Taiwen Huang, Yuhua Xiong, Aimin Yang, Zhilong Zhao, Rong Zhang and Jinshan Li: Proc. 10th Int. Symp. on Superalloys, ed. by K. A. Green, T. M. Pollock, H. Harada,T. E. Howson, R. C. Reed, J. J. Schirra and S. Walston, (TMS, Warrendale, PA, 2004) pp. 493–500.
9) J. R. Kattus: *Aerospace Structural Metals Handbook*, (Purdue Research Foundation, West Lafayette, Indiana, 1999) Code 4218, p. 2.
10) C. T. Sims, N. S. Stoloff and W. C. Hagel: *Superalloys II*, (John Wiley & Sons, New York, 1987) pp. 66–94.
11) J. Rüusing, N. Wanderka, U. Czubayko, V. Naundorf, D. Mukherji and J. Rösler: Scr. Mater. **46** (2002) 235–240.
12) M. V. Acharya and G. E. Fuchs: Mater. Sci. Eng. A **381** (2004) 143–153.
13) K. Durst and M. Göken: Mater. Sci. Eng. A **387–389** (2004) 312–316.
14) G. E. Fuchs: Mater. Sci. Eng. A **300** (2001) 52–60.
15) S. Wöllmer, T. Mack and U. Glatzel: Mater. Sci. Eng. A **319–321** (2001) 792–795.
16) A. F. Giamei and D. L. Anton: Metall. Trans. A **16A** (1985) 1997–2005.
17) R. Burgel, J. Grossmann, O. Lusebrink, H. Mughrabi, F. Pyczak, R. F. Singer and A. Volek: Proc. 10th Int. Symp. on Superalloys, ed. by K. A. Green, T. M. Pollock, H. Harada, T. E. Howson, R. C. Reed, J. J. Schirra and S. Walston, (TMS, Warrendale, PA, 2004) pp. 25–34.
18) C. M. F. Rae and R. C. Reed: Acta Metall. **49** (2001) 4113–4125.
19) J. X. Yang, Q. Zheng, X. F. Sun, H. R. Guan and Z. Q. Hu: Mater. Sci. Eng. A **67** (2007) 100–108.
20) S. Tin and T. M. Pollock: Mater. Sci. Eng. A **348** (2003) 111–121.
21) A. C. YEH and S. TIN: Metall. Trans. A **37A** (2006) 2621–2631.
22) C. T. Sims, N. S. Stoloff and W. C. Hagel: *Superalloys II*, (John Wiley & Sons, New York, 1987) pp. 117–118.
23) E. V. Monastyrskaia, E. V. Petrov, V. E. Beljaev and A. M. Dushkin: Proc. 10th Int. Symp. on Superalloys, ed. by K. A. Green, T. M. Pollock, H. Harada, T. E. Howson, R. C. Reed, J. J. Schirra and S. Walston, (TMS, Warrendale, PA, 2004) pp. 779–786.
24) R. A. Hobbs, S. Tin, C. M. F. Rae, R. W. Broomfield and C. J. Humphreys: Proc. 10th Int. Symp. on Superalloys, ed. by K. A. Green, T. M. Pollock, H. Harada, T. E. Howson, R. C. Reed, J. J. Schirra and S. Walston, (TMS, Warrendale, PA, 2004) pp. 819–825.
25) R. E. Reed-Hill and R. Abbaschian: *Physical Metallurgy Principles*, (PWS Publishing Company, Boston, 1994) pp. 434–436.
26) J. S. Hou and J. T. Guo: J. Mater. Eng. Perform **15** (2006) 67–75.
27) P. J. Warren, A. Cerezo and G. D. W. Smith: Mater. Sci. Eng. A **250** (1998) 88–92.
28) A. Volek, F. Pyczak, R. F. Singer and H. Mughrabi: Scr. Mater. **52** (2005) 141–145.
29) L. J. Carroll, Q. Feng, J. F. Mansfield and T. M. Pollock: Metall. Trans. A **37A** (2006) 2927–2938.
30) C. T. Sims, N. S. Stoloff and W. C. Hagel: *Superalloys II*, (John Wiley & Sons, New York, 1987) pp. 111–116.
31) C. T. Sims, N. S. Stoloff and W. C. Hagel: *Superalloys II*, (John Wiley & Sons, New York, 1987) p. 78.